



## OPTIMIZATION OF NMC811 SYNTHESIS VIA OXALATE COPRECIPIATION METHOD FOR LITHIUM-ION BATTERY CATHODE

Fiona Angellinnov<sup>a</sup>, Achmad Subhan<sup>b</sup>, Bambang Priyono<sup>a,c</sup>, Anne Zulfia Syahrial<sup>a,c,\*</sup>

<sup>a</sup>Department of Metallurgical and Materials Engineering, University of Indonesia  
Kampus UI, Kukusan, Depok, Indonesia 16424

<sup>b</sup>Research Center for Advanced Materials, National Research and Innovation Agency (BRIN)  
B.J. Habibie Sains and Technology Area, Banten, Indonesia 15314

<sup>c</sup>Tropical Renewable Energy Centre, University of Indonesia  
Kampus UI, Kukusan, Depok, Indonesia 16424

\*E-mail: anne.zulfia@ui.ac.id

Received: 30-08-2024, Revised: 14-10-2024, Accepted: 21-10-2024

### Abstract

*NMC811 was synthesized through the oxalate coprecipitation method, followed by the solid-state method of lithiation. Stirring speed (500, 750, 1000 rpm), aging time (0, 3, 5h), sintering atmosphere (with and without oxygen flow), sintering temperature (700, 750, 800 °C), and lithium concentration (0, 2, 5% excess) effect on the NMC811 were examined. Characterization results showed that the optimum stirring speed and aging time are 750 rpm and 3 hours. Based on structural analysis, the best condition for sintering is in oxygen atmospheres at 800 °C with a lithium concentration of 2% excess. NMC811, synthesized with these optimum parameters, provided a 212.93 mAh/g capacity. These findings deliver insight into NMC811 synthesis optimization.*

**Keywords:** Cathode material, oxalate coprecipitation, NMC811, synthesis method

## 1. INTRODUCTION

Lithium-ion batteries are commonly used in portable electronic devices such as laptops, mobile phones, and electric vehicles [1]. The price and performance of a LIB are determined by its active cathode material [2]. Among the cathode materials, nickel manganese cobalt ( $\text{LiNi}_x\text{Mn}_y\text{Co}_z\text{O}_2$ , NMC) is known to have high specific capacity and operational voltage [3]. Compared to the other types of NMC, NMC811 ( $\text{LiNi}_{0.8}\text{Mn}_{0.1}\text{Co}_{0.1}\text{O}_2$ ) possesses the highest specific capacity of about ~160-200 mAh/g, whereas at the same time, it is cheaper due to its lower cobalt content, but with high electric potential [4].

However, the high nickel content in NMC811 leads to a high degree of cation mixing between  $\text{Ni}^{2+}$  and  $\text{Li}^+$ , resulting in capacity fade and phase change [5]. In addition, exposure of NMC811 to

air forms impurities in the form of  $\text{Li}_2\text{CO}_3$  and  $\text{LiOH}$  on its surface, causing defluorination of the binder, gas release, reacting with the electrolyte, and irreversible phase transition, thus lowering the electrochemical performance [6]-[9]. Since the electrochemical performance of NMC811 depends on crystallinity, phase purity, particle size, and structure [10]-[11]. The synthesis process of NMC811 needs to be optimized.

NMC811 can be synthesized through several methods, such as spray drying [12], sol-gel [13], hydrothermal [14], solid state [15], solution combustion [16], and coprecipitation [17]. Among the methods, coprecipitation has many advantages, such as low temperature, precise stoichiometric proportions, homogenous mixing, and ease of scalability and morphology control, thus making it the most widely used synthesis method [18]-[19]. The coprecipitation method can be classified into hydroxide coprecipitation,

DOI: 10.55981/metalurgi.2024.759

© 2024 Author(s). This is an open access article under the CC BY-SA license (<http://creativecommons.org/licenses/by-sa/4.0>)

Metalurgi is Sinta 2 Journal (<https://sinta.kemdikbud.go.id/journals/profile/3708>) accredited by Ministry of Education, Culture, Research, and Technology, Republic Indonesia

carbonate coprecipitation, and oxalate coprecipitation [20]. Oxalate coprecipitation is cheaper and environmentally friendlier than hydroxide coprecipitation because it uses oxalic acid as a precipitating and complexing agent and does not require an inert atmosphere [21]. The precipitate is mixed with a lithium source, followed by heat treatment to obtain the final NMC [22].

Oxalate coprecipitation has been used to synthesize NMC [22]-[24]. NMC811 was synthesized by Wu et al. [21] using metal chloride salts precipitated by oxalic acid, followed by lithiation using a 1% excess lithium source. The NMC811 showed  $I_{(003)}/I_{(104)}$  of 1.46 with a 200-300 nm particle size. The material provided a capacity and charge transfer resistance of 180 mAh/g and 68  $\Omega$ , respectively. Wijareni et al., [25] used sulfate metal salts to synthesize NMC811 via oxalate coprecipitation. Their results showed a circular particle with an average size of 17.16  $\mu\text{m}$  with initial capacity, initial efficiency, conductivity, and lithium-ion diffusion of 178.93 mAh/g, 94.32%,  $1.20 \times 10^{-7}$ , and  $4.22 \times 10^{-9}$ , respectively. In their work, Gustiana et al., [26] used oxalate coprecipitation and compared it with hydroxide coprecipitation. Both methods resulted in spherical asymmetrical particles with a size <1 micron. They obtained that the NMC811 synthesized using oxalate coprecipitation provided higher capacity (102.42 mAh/g) than hydroxide coprecipitation (79.90 mAh/g).

In this work, NMC811 was synthesized through the oxalate coprecipitation method using metal nitrate precursors. The effects of synthesis parameters such as stirring speed, aging time, lithium amount, sintering temperature, and atmosphere were examined. To the best of the authors' knowledge, no article has reported on these synthesis parameters using the oxalate coprecipitation method. The results are given and discussed in detail in the following session.

## 2. MATERIALS AND METHODS

### 2.1 Optimization of NMC811 Synthesis

The chemicals were lithium hydroxide monohydrate ( $\text{LiOH}\cdot\text{H}_2\text{O}$ ), nickel (II) nitrate hexahydrate ( $\text{Ni}(\text{NO}_3)_2\cdot 6\text{H}_2\text{O}$ ), manganese (II) nitrate tetrahydrate ( $\text{Mn}(\text{NO}_3)_2\cdot 4\text{H}_2\text{O}$ ), cobalt (II) nitrate hexahydrate ( $\text{Co}(\text{NO}_3)_2\cdot 6\text{H}_2\text{O}$ ), and oxalic acid ( $\text{H}_2\text{C}_2\text{O}_4$ ), all were purchased from Sigma-Aldrich and used without any further treatment and or purification. A stoichiometric amount (8:1:1) of  $\text{Ni}(\text{NO}_3)_2\cdot 6\text{H}_2\text{O}$ ,  $\text{Mn}(\text{NO}_3)_2\cdot 4\text{H}_2\text{O}$ , and  $\text{Co}(\text{NO}_3)_2\cdot 6\text{H}_2\text{O}$  were dissolved into distilled water. An equimolar  $\text{H}_2\text{C}_2\text{O}_4$  was also dissolved in a separate beaker in distilled water. The metal salt

mixture was stirred at 60°C at three different stirring speeds (500, 750, 1000 rpm) while titrated with oxalic acid solution. The mixture was then stirred for another 2 h, without aging (aging 0 h). The mixture was then filtered, and the NMC-oxalate precipitate was dried. The three samples were labeled S-500, S-750, and S-1000, corresponding to their stirring speed. The best stirring speed was then used to determine the aging time of 0, 3, and 5 h, and the samples were labeled as A-0, A-3, and A-5, respectively. The process is illustrated in Fig. 1(a).

The best NMC-oxalate precursor sample with optimum stirring speed and aging time was then chosen to be further lithiated with  $\text{LiOH}\cdot\text{H}_2\text{O}$  through the wet milling method (300 rpm for 1 h) followed by sintering for 12 h, illustrated in Fig. 1(b). Two sintering atmospheres at 750 °C (with and without oxygen flow) with a fixed amount of lithium (5% excess) were applied, and the samples were labeled as LNMC-oxy and LNMC-air, respectively. The best sintering atmosphere was then used for the temperature variation of 700, 750, and 800 °C, labeled as LNMC-700, LNMC-750, and LNMC-800. The best sintering atmosphere and temperature were then applied for variations of lithium amount of 0, 2, and 5% excess and labeled LNMC-0, LNMC-2, and LNMC-5. The best LNMC sample, labeled as LNMC811, was then tested for electrochemical performance.

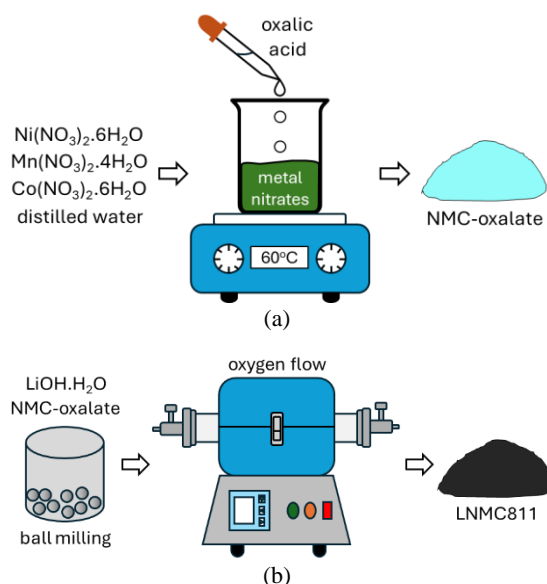


Figure 1. (a) Schematic of NMC-oxalate precursor synthesis process, and (b) lithiation of NMC-oxalate with lithium source

### 2.2 Characterization

Samples were characterized using Infrared spectroscopy (FTIR, Perkin Elmer) to ensure no oxalate compound remains. X-ray diffraction

(XRD, PANalytical X'Pert PRO, K- $\alpha$  Cu of 1.54 Å) in the  $2\theta$  range of  $10^\circ$ – $90^\circ$  was used to analyze the crystal structure and the phase formed. Thermogravimetry analysis (TGA, LabSys Evo) examined thermal behaviour. In contrast, a field emission scanning electron microscope with energy dispersive X-ray spectroscopy (FESEM/EDS, FEI Inspect F-50) was used for surface morphology and elemental analysis. The

electrochemical performance was carried out using electrochemical impedance spectroscopy in the frequency range of 0.1–50 kHz at 100 mV (EIS, Metrohm Autolab PGSTAT 302 N) and charge-discharge (CD, Wonatech, CCJ8F2-8 PS) to examine the conductivity and capacity, respectively.

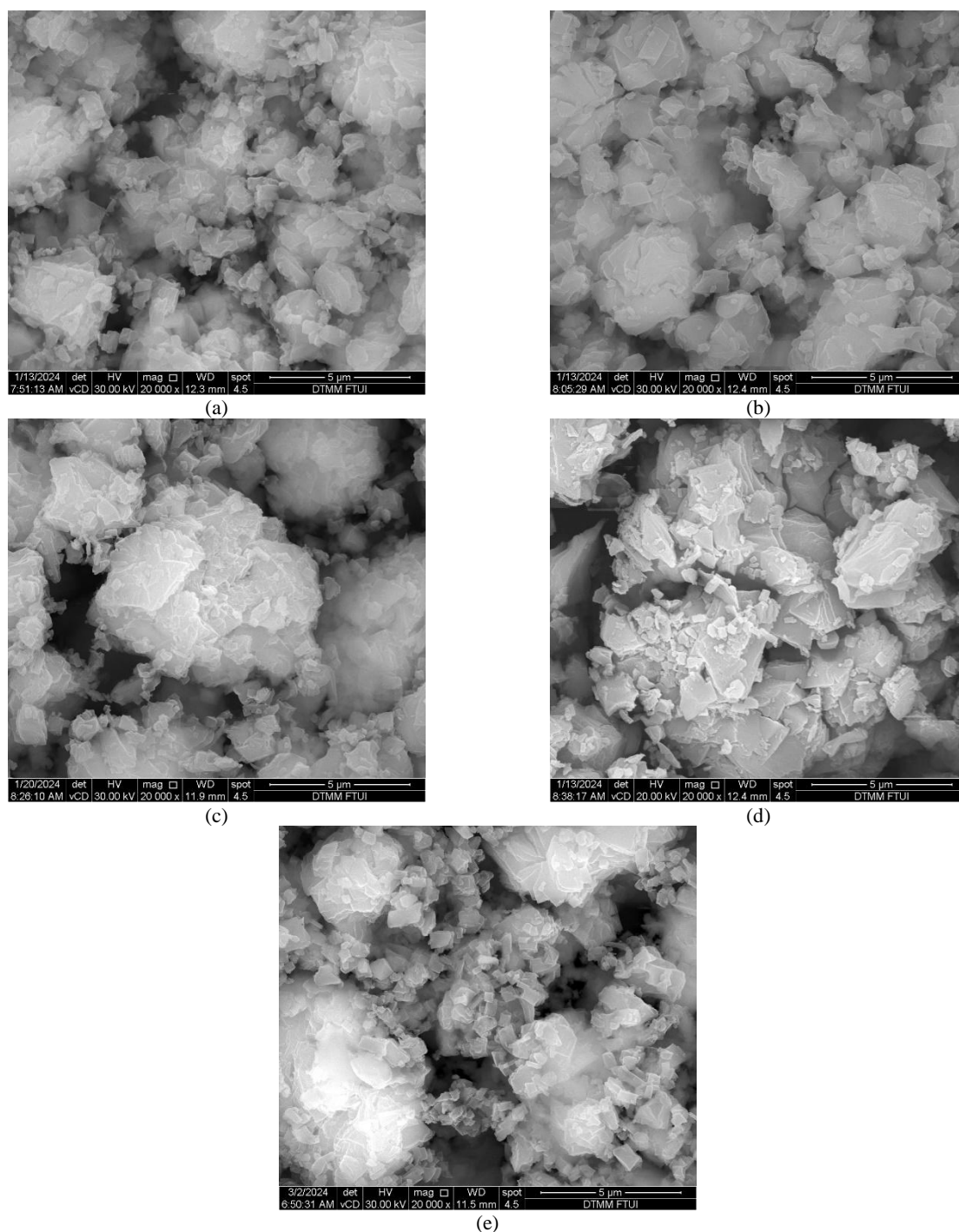


Figure 2. Electron images of (a) S-500, (b) S-750, (c) S-1000, (d) A-3, and (e) A-5

### 3. RESULTS AND DISCUSSION

#### 3.1 Characteristics of NMC-oxalate

The resulting NMC-oxalate powder synthesized with different stirring speeds was characterized using FESEM (field emission scanning electron microscopy), and the results are shown in Figs. 2(a)-2(c). In contrast, the particle size analysis is listed in Table 1. The electron images show that the particles are irregularly shaped primary particles. Increasing the stirring speed from 500 to 750 rpm reduces the particle size from 0.96 to 0.77  $\mu\text{m}$ . However, when the speed is increased to 1000 rpm, the particles are agglomerated with a size of 2.51  $\mu\text{m}$ . This agglomeration is due to the accelerated collision among the particles [20]. Based on the FESEM results, the sample S-750 (stirring at 750 rpm with 0h aging time) has the smallest particle size and was chosen for the next variation in aging time. The reason is that the contact area between the electrode and electrolyte is increased, and the distance of  $\text{Li}^+$  diffusion is reduced with a smaller particle size, thus increasing the electrochemical performance [26]-[27]. The morphologies of A-3 and A-5 (3 and 5h aging time, respectively) are shown in Figs. 2(d)-2(e). Analysis of the particle size (Table 1) determines that the aging time of 3 h (sample A-3) has the smallest size of 0.71, compared to A-5 and S-750 (1.02 and 0.77, respectively). Therefore, the best aging time obtained is 3 h.

Table 1. Average particle size of S-500, S-750, S-1000, A-3, A-5

Sample	Average particle size ( $\mu\text{m}$ )
S-500	0.96
S-750	0.77
S-1000	2.51
A-3	0.71
A-5	1.02

Characterization using infrared was conducted, and the spectra are shown in Fig. 3 (a). All samples show absorption at 3400 and 1615  $\text{cm}^{-1}$  wavenumber, corresponding to O-H stretching and bending vibrations, respectively [28]. The 1315 and 1310  $\text{cm}^{-1}$  peaks indicate the C-O groups [26]. Absorption around 823, 750, and 745  $\text{cm}^{-1}$  is due to C-O and O-C=O bonds [29]. Metal oxalate is detected at wavenumber 485  $\text{cm}^{-1}$  [30]. These results reveal information that the complexation of metal oxalate has been successfully carried out.

Sample A-3 with optimum conditions (750 rpm and 3h aging time) was further thermally analyzed before and after mixing with  $\text{LiOH}\cdot\text{H}_2\text{O}$ , and the result is shown in Fig. 3(b). For sample A-3, heating to a temperature of 280°C before lithiation results in a weight loss of 20%. This corresponds

to the release of two water molecules from the NMC precursor, confirming that the coprecipitation between metal nitrates and oxalic acid results in metal oxalate dihydrate following the path in Eq. 1 [23].

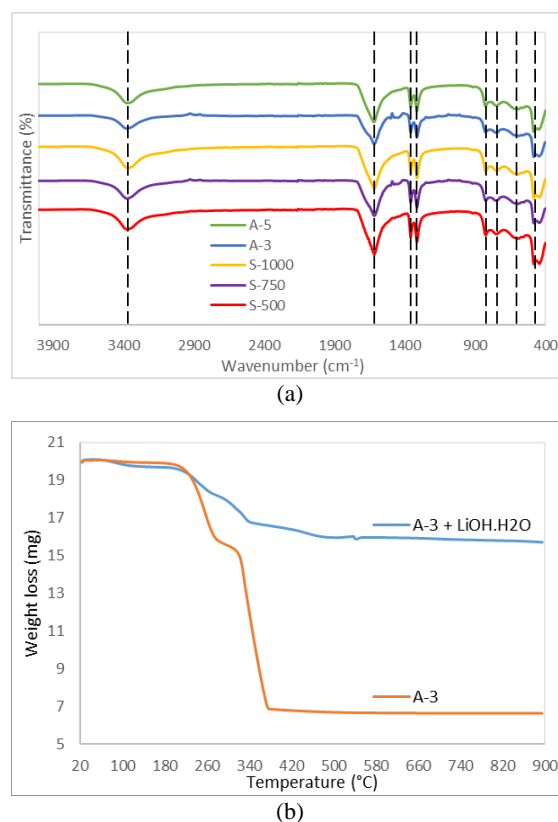
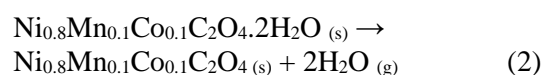
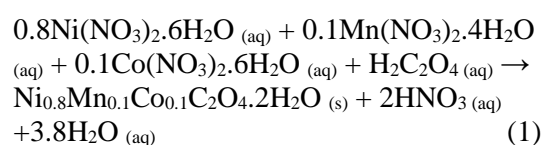
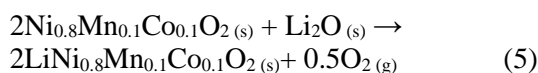
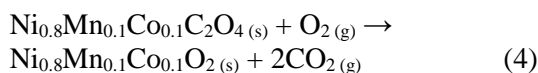
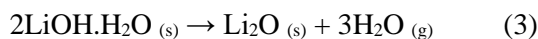


Figure 3. (a) Infrared spectra of S-500, S-750, S-1000, A-3, A-5, and (b) thermal analysis of A-3 sample before and after lithiation with  $\text{LiOH}\cdot\text{H}_2\text{O}$

The following weight loss of 57% at 380  $^{\circ}\text{C}$  from sample A-3 before lithiation is attributed to removing gaseous species from the precursor [31]. After 400  $^{\circ}\text{C}$ , no significant weight loss was detected. After lithiation, sample A-3 shows weight loss of 1.57, 7.14, 8.51, and 4.50% from room temperature to 180, 180-270, 270-350, and 350-490  $^{\circ}\text{C}$ , respectively. The loss of adsorbed water from NMC-oxalate and  $\text{LiOH}\cdot\text{H}_2\text{O}$  is for the first and second weight loss, the third is the reaction between NMC-oxalate and oxygen, and the last one is the formation of the final NMC following the path given in Eqs. 2-5 [32]-[34]. Similar results were also observed in another study [27].





### 3.2 Characteristics of NMC811

In the thermal analysis, the lithiated NMC-oxalate was sintered in two conditions, with and without oxygen flow. In Figure 4 (a), LNMC-air and LNMC-oxy show similar spectra with small absorption at 880 and 1400  $\text{cm}^{-1}$ . These can be attributed to incomplete burning of oxalate or the formation of  $\text{Li}_2\text{CO}_3$  impurities due to excess lithium [29].

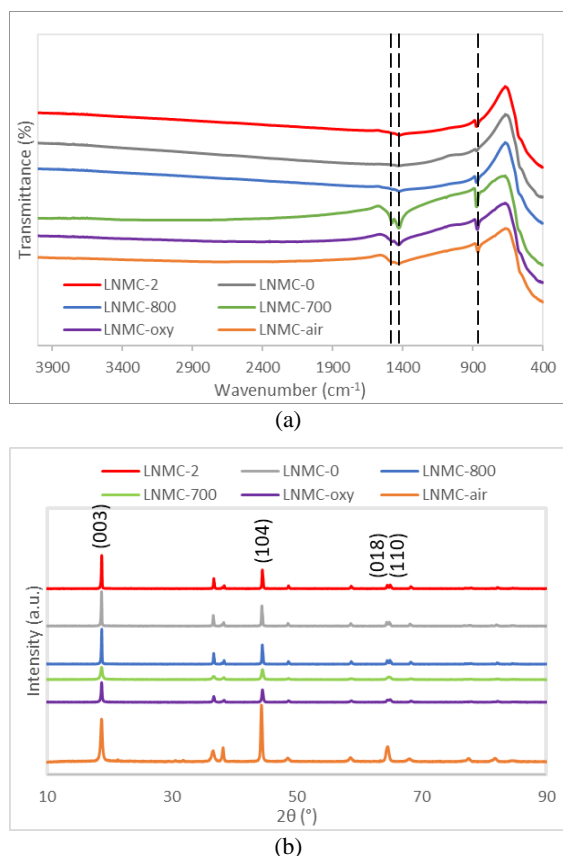


Figure 4. (a) Infrared spectra and (b) X-ray diffractograms of LNMC samples

Further characterization using XRD was conducted to confirm this proposition. Analysis of the X-ray diffractograms of all LNMC samples except LNMC-air (shown in Fig. 4(b)) match with reference ICDD 01-070-4314 (lithium nickel manganese cobalt oxide with layered rhombohedral structure and R-3m space group) with no impurities detected. However, LNMC-air

matches with lithium nickel oxide (reference 01-077-2126), showing that manganese and cobalt were not incorporated into the structure. These results show that oxygen is important in the sintering process of NMC811, primarily because of the lower bonding energy between  $\text{Ni}^{3+}$  and  $\text{O}^{2-}$ , resulting in oxygen loss from the nickel-rich material structure during the sintering process [35]-[36].

LNMC-air and LNMC-oxy samples analyzed using FESEM (Figs. 5(a)-5(b)) show semicircular-shaped particles with an average particle size of 61 nm and 69 nm (Table 2), respectively.

Based on the characterization results, the sintering condition with oxygen flow was then used to determine the sintering temperature. Infrared spectra shown in Fig. 4(a), purple, green, and blue lines correspond to the sintering temperatures of 700, 750, and 800 $^{\circ}\text{C}$ , respectively. The sample sintered at 700 $^{\circ}\text{C}$  shows a sharper absorption around 880 and 1400  $\text{cm}^{-1}$ . There is a possibility that, because of the low sintering temperature, the removal of oxalate from the structure is incomplete. This can also be observed from the FESEM image in Fig. 5(c), which shows irregular particles (51 nm) compared to the particles sintered at 750 and 800 $^{\circ}\text{C}$  that are semicircular (69 and 58 nm) (Figs. 5(b)-5(d)). Further, the XRD results in Fig. 4(b) confirm that LNMC-700 shows no clear peak splitting (018)/(110) and has a low-intensity ratio of peak (003)/(104), which is only 1.16. The clear peak (018)/(110) splitting and I(003)/I(104) ratio higher than 1.20 are indications of a well-ordered layered structure and low cation mixing [37]-[38]. Sintering at 800 $^{\circ}\text{C}$  resulted in a high I(003)/I(104) of 1.67, higher than 750 $^{\circ}\text{C}$  (1.47). It can then be concluded that the optimum sintering temperature is 800 $^{\circ}\text{C}$ .

The effect of lithium concentration is investigated by conducting the sintering process under an oxygen atmosphere at 800 $^{\circ}\text{C}$ , with a variation of 0, 2, and 5% excess lithium. The electron images in Figs. 5(d)-5(f) show that all samples possess semicircular particles with the smallest particle size of 57 nm for the LNMC-2 sample. Infrared results of these samples show little absorption around 880 and 1400  $\text{cm}^{-1}$  compared to other LNMC samples, meaning that the removal of oxalate is completed and no impurities of lithium compounds. This is confirmed by XRD characterization. The highest I<sub>(003)</sub>/I<sub>(104)</sub> ratio is exhibited by sample LNMC-2 (Table 2), which is 1.70.

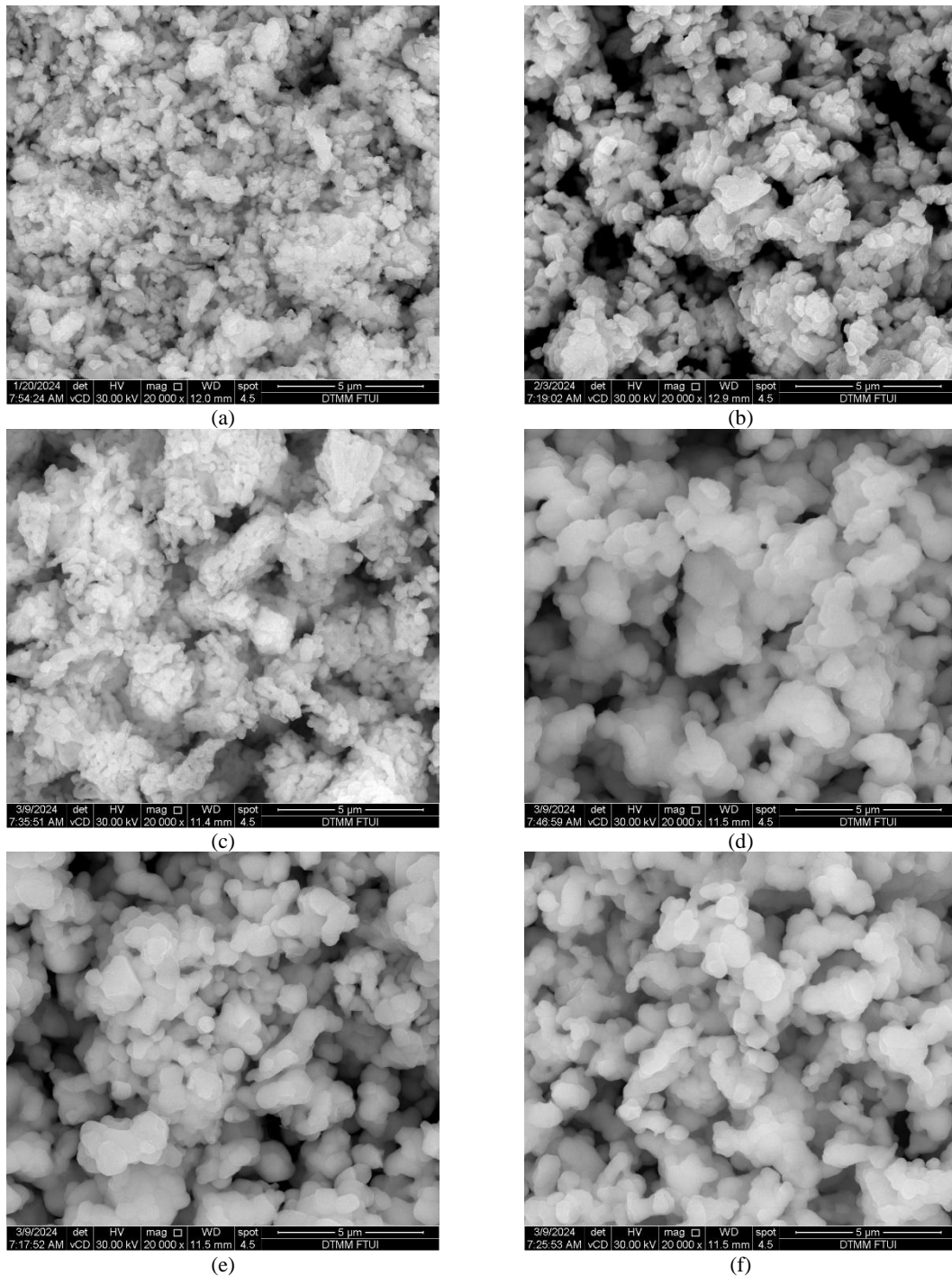


Figure 5. Electron images of (a) LNMCM-air, (b) LNMCM-oxy, (c) LNMCM-700, (d) LNMCM-800, (e) LNMCM-0, and (f) LNMCM-2

In conclusion, the optimum parameters are using 2% excess lithium, sintering temperature at 800°C under oxygen flow. This sample is then labeled as LNMCM811 and characterized using EDS. The detected elements listed in Table 3 show that the nickel, manganese, and cobalt ratio confirms the amount used in the synthesis. Figure 6(a) shows the EIS result of the LNMCM811 sample. Equation 1 is used to calculate the conductivity ( $\Omega$ ), where  $l$  is the thickness (150  $\mu\text{m}$ ) and  $A$  is the area (2.14  $\text{cm}^2$ ) of the sample. The charge transfer resistance ( $R_{ct}$ ) measured for the LNMCM811 sample is 261.4  $\Omega$ , resulting in a  $2.68 \times 10^{-5}$  S/cm conductivity. This result is

similar to the result from another study [16]. The charge-discharge graph in Fig. 6(b) shows the initial charge and discharge capacity of LNMCM811 (229.73 and 212.93 mAh/g, respectively) with a coulombic efficiency of 92.68%. The discharge capacity of this work is higher compared to other studies conducted by Wu et al. (discharge capacity of 178 mAh/g) [21], Wijareni et al. (178.93 mAh/g) [25], and Gustiana et al. (102.42 mAh/g) [26]. Figure 6(a) shows the EIS result of the LNMCM811 sample. Equation 1 is used to calculate the conductivity ( $\Omega$ ), where  $l$  is the thickness (150  $\mu\text{m}$ ) and  $A$  is the area (2.14  $\text{cm}^2$ ) of the sample.

Table 2. Average particle size and I(003)/I(104) of LNMC samples

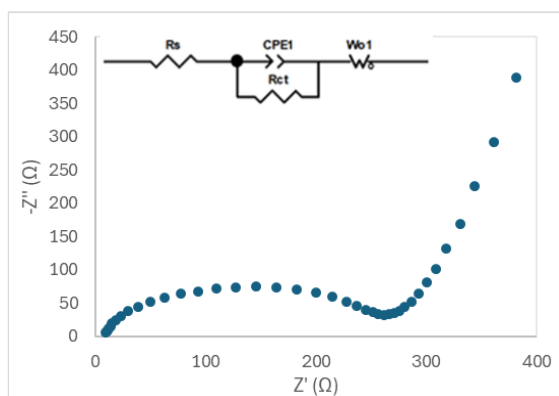
Sample	Lithium amount	Sintering temperature (°C)	Average particle size (nm)	I(003)/I(104)
LNMC-air			61	0.78
LNMC-oxy (LNMC-750)	5% excess	750	69	1.47
LNMC-700		700	51	1.16
LNMC-800 (LNMC-5)		800	58	1.67
LNMC-0	0% excess		60	1.61
LNMC-2	2% excess		57	1.70

The charge transfer resistance ( $R_{ct}$ ) measured for the LNMC811 sample is 261.4  $\Omega$ , resulting in a  $2.68 \times 10^{-5}$  S/cm conductivity.

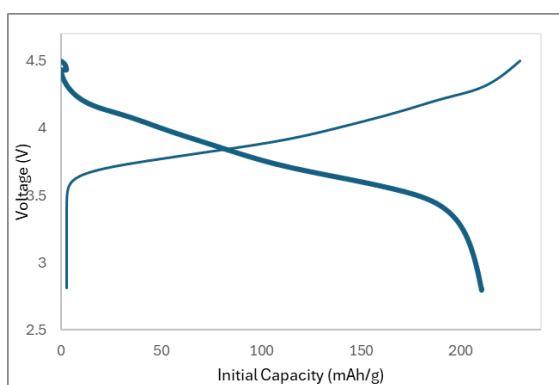
Table 3. Elemental composition of LNMC811

Element (wt.%)	Ni	Mn	Co	O
LNMC811	57.95	4.98	8.96	28.11

This result is similar to the result from another study [16].



(a)



(b)

Figure 6. (a) Nyquist plot, (b) initial charge-discharge capacity of LNMC811

The charge-discharge graph in Fig. 6(b) shows the initial charge and discharge capacity of LNMC811 (229.73 and 212.93 mAh/g, respectively) with a coulombic efficiency of 92.68%. The discharge capacity of this work is

higher compared to other studies conducted by Wu et al. (discharge capacity of 178 mAh/g) [21], Wijareni et al. (178.93 mAh/g) [25], and Gustiana et al. (102.42 mAh/g) [26].

## 4. CONCLUSION

This study examined the synthesis parameters such as stirring speed, aging time, lithium amount, sintering atmosphere, and temperature to determine the optimum parameters for NMC811 synthesis. Increasing stirring speed (750 rpm) and aging time (3 hours) in the synthesis of NMC811 oxalate precursor resulted in a smaller particle size of 0.71  $\mu\text{m}$ . Lithium amount (2% excess) and sintering conditions (800  $^{\circ}\text{C}$  under oxygen flow) are important to obtain the crystalline structure with low cation mixing and impurities. These optimum conditions result in high electrochemical performance of NMC811 with a coulombic efficiency of 92.68% and a 212.93 mAh/g capacity. These results are promising for the synthesis of NMC811 with a simple and cheap process that does not require an inert atmosphere.

## ACKNOWLEDGMENT

This research is funded by the Indonesian Endowment Fund for Education (LPDP) on behalf of the Indonesian Ministry of Education, Culture, Research, and Technology, and managed under the INSPIRASI Program (Contract No. 6635/E3/KL.02.02/2023)

## REFERENCES

- [1] R. Sharma, H. Kumar, G. Kumar, S. Sharma, R. Aneja, A. K. Sharma, R. Kumar, and P. Kumar, "Progress and challenges in electrochemical energy storage devices: Fabrication, electrode material, and economic aspects," *Chemical Engineering Journal*, vol. 468, p. 143706, 2023. DOI: 10.1016/j.cej.2023.143706.
- [2] J. Yang, X. Liang, H. Ryu, C. S. Yoon, and Y. Sun, "Ni-rich layered cathodes for lithium-ion batteries : From challenges to the future," *Energy Storage Mater.*, vol. 63, p. 102969, 2023. DOI: 10.1016/j.ensm.2023.102969.
- [3] B. Xiao and X. Sun, "Surface and subsurface reactions of Lithium transition metal oxide cathode materials: An overview of the fundamental origins and remedying approaches," *Adv Energy*

- Mater.*, vol. 8, no. 29, pp. 1-27, 2018. DOI: 10.1002/aenm.201802057.
- [4] J. V. Laveda, J. E. Low, F. Pagani, E. Stilp, S. Dilger, V. Baran, M. Heere, and C. Battaglia, "Stabilizing capacity retention in NMC811/graphite full cells via TMSPi Electrolyte Additives," *ACS Appl Energy Mater.*, vol. 2, no. 10, pp. 7036-7044, 2019. DOI: 10.1021/acsaem.9b00727.
- [5] P. Yan, J. Zheng, L. Dongping, Y. Wei, J. Zheng, Z. Wang, S. Kuppan, J. Yu, L. Luo, D. Edwards, M. Olszta, K. Amine, J. Liu, J. Xiao, F. Pan, G. Chen, J. G. Zhang, and C. M. Wang, "Atomic-resolution visualization of distinctive chemical mixing behavior of Ni, Co, and Mn with Li in layered Lithium transition-metal oxide cathode materials," *Chemistry of Materials*, vol. 27, no. 15, pp. 5393-5401, 2015. DOI: 10.1021/acs.chemmater.5b02016.
- [6] S. T. Myung, F. Maglia, K. J. Park, C. S. Yoon, P. Lamp, S. J. Kim, and Y. K. Sun, "Nickel-rich layered cathode materials for automotive Lithium-ion batteries: Achievements and perspectives," *ACS Energy Letters*, vol. 2, no. 1, pp. 196-223, 2017. DOI: 10.1021/acseenergylett.6b00594.
- [7] S. E. Renfrew and B. D. McCloskey, "Residual Lithium carbonate predominantly accounts for first cycle CO<sub>2</sub> and CO outgassing of Li-stoichiometric and Li-rich layered transition-metal oxides," *J Am Chem Soc.*, vol. 139, no. 49, pp. 17853-17860, 2017. DOI: 10.1021/jacs.7b08461.
- [8] Y. Bi, T. Wang, M. Liu, R. Du, W. Yang, Z. Liu, Z. Peng, Y. Liu, D. Wang, and X. Sun, "Stability of Li<sub>2</sub>CO<sub>3</sub> in cathode of lithium ion battery and its influence on electrochemical performance," *RSC Adv.*, vol. 6, no. 23, pp. 19233-19237, 2016. DOI: 10.1039/c6ra00648e.
- [9] A. Manthiram, J. C. Knight, S. T. Myung, S. M. Oh, and Y. K. Sun, "Nickel-rich and Lithium-rich layered oxide cathodes: Progress and perspectives," *Adv Energy Mater.*, vol. 6, no. 1, 2016. DOI: 10.1002/aenm.201501010.
- [10] H. Zhang, H. Zhao, M. A. Khan, W. Zou, J. Xu, L. Zhang, and J. Zhang, "Recent progress in advanced electrode materials, separators and electrolytes for lithium batteries," *J Mater Chem A Mater.*, vol. 6, p. 20564, 2018. DOI: 10.1039/c8ta05336g.
- [11] L. J. Li, X. H. Li, Z. X. Wang, H. J. Guo, P. Yue, W. Chen, and L. Wu, "A simple and effective method to synthesize layered LiNi<sub>0.8</sub>Co<sub>0.1</sub>Mn<sub>0.1</sub>O<sub>2</sub> cathode materials for lithium ion battery," *Powder Technol.*, vol. 206, pp. 353-357, 2011. DOI: 10.1016/j.powtec.2010.09.010.
- [12] B. Lin, Z. Wen, Z. Gu, and S. Huang, "Morphology and electrochemical performance of Li[Ni<sub>1/3</sub>Co<sub>1/3</sub>Mn<sub>1/3</sub>O<sub>2</sub>] cathode material by a slurry spray drying method," *J Power Sources*, vol. 175, no. 1, pp. 564-569, 2008. DOI: 10.1016/j.jpowsour.2007.09.055.
- [13] J. Xu, S. L. Chou, Q. F. Gu, H. K. Liu, and S. X. Dou, "The effect of different binders on electrochemical properties of LiNi<sub>1/3</sub>Mn<sub>1/3</sub>Co<sub>1/3</sub>O<sub>2</sub> cathode material in Lithium ion batteries," *J Power Sources*, vol. 225, pp. 172-178, 2013. DOI: 10.1016/j.jpowsour.2012.10.033.
- [14] Q. Jing, J. Zhang, C. Yang, Y. Chen, and C. Wang, "A novel and practical hydrothermal method for synthesizing LiNi<sub>1/3</sub>Co<sub>1/3</sub>Mn<sub>1/3</sub>O<sub>2</sub> cathode material," *Ceram Int.*, vol. 46, no. 12, pp. 20020-20026, 2020. DOI: 10.1016/j.ceramint.2020.05.073.
- [15] L. Tang, X. Cheng, R. Wu, T. Cao, J. Lu, Y. Zhang, and Z. Zhang, "Monitoring the morphology evolution of LiNi<sub>0.8</sub>Mn<sub>0.1</sub>Co<sub>0.1</sub>O<sub>2</sub> during high-temperature solid state synthesis via in situ SEM," *Journal of Energy Chemistry*, vol. 66, pp. 9-15, 2022. DOI: 10.1016/j.jechem.2021.07.021.
- [16] F. Angellinnov, A. Subhan, A. J. Drew, and A. Z. Syahrial, "Synthesis of Sn doped and rice husk derived activated carbon surface coating NMC 811 through solution combustion method," *Heliyon*, vol. 10, no. 1, p. e23199, 2024. DOI: 10.1016/j.heliyon.2023.e23199.
- [17] A. L. Lipson, B. J. Ross, J. L. Durham, D. Liu, M. Leresche, T. T. Fister, L. Liu, and K. Kim, "Stabilizing NMC 811 Li-ion battery cathode through a rapid coprecipitation process," *Applied Energy Materials*, vol. 4, pp. 1972-1977, 2021. DOI: 10.1021/acsaem.0c03112.
- [18] X. Zhao, J. Wang, X. Dong, G. Liu, W. Yu, and L. Wang, "Structure design and performance of LiNi<sub>x</sub>Co<sub>y</sub>Mn<sub>1-x-y</sub>O<sub>2</sub> cathode materials for lithium-ion batteries: A review," *Journal of the*

- Chinese Chemical Society*, vol. 61, no. 10, pp. 1071-1083, 2014. DOI: 10.1002/jccs.201400107.
- [19] H. Li, Q. Xu, X. X. Shi, D. W. Song, and L. Q. Zhang, "Electrochemical performance of  $\text{LiNi}_0.5\text{Mn}_0.5\text{O}_2$  with different synthesis methods," *Rare Metals*, vol. 34, no. 8, pp. 580-585, 2015. DOI: 10.1007/s12598-013-0088-z.
- [20] M. Malik, K. H. Chan, and G. Azimi, "Review on the synthesis of  $\text{LiNi}_x\text{Mn}_y\text{Co}_{1-x-y}\text{O}_2$  (NMC) cathodes for lithium-ion batteries," *Mater Today Energy*, vol. 28, p. 101066, 2022. DOI: 10.1016/j.mtener.2022.101066.
- [21] C. Y. Wu, Q. Bao, Y. T. Tsai, and J. G. Duh, "Tuning (003) interplanar space by boric acid co-sintering to enhance  $\text{Li}^+$  storage and transfer in  $\text{Li}(\text{Ni}_0.8\text{Co}_0.1\text{Mn}_0.1)\text{O}_2$  cathode," *J Alloys Compd*, vol. 865, p. 158806, 2021. DOI: 10.1016/j.jallcom.2021.158806.
- [22] H. Tian, N. Ye, D. Liu, and W. Li, "Effects of synthesis conditions on the structural and electrochemical properties of layered  $\text{LiNi}_{1/3}\text{Co}_{1/3}\text{Mn}_{1/3}\text{O}_2$  cathode material via oxalate coprecipitation method," *Rare Metals*, vol. 27, no. 6, pp. 575-579, 2008. DOI: 10.1016/S1001-0521(08)60185-0.
- [23] C. F. Zhang, P. Yang, X. Dai, X. Xiong, J. Zhan, and Y. L. Zhang, "Synthesis of  $\text{LiNi}_{1/3}\text{Co}_{1/3}\text{Mn}_{1/3}\text{O}_2$  cathode material via oxalate precursor," *Transactions of Nonferrous Metals Society of China (English Edition)*, vol. 19, no. 3, pp. 635-641, 2009. DOI: 10.1016/S1003-6326(08)60325-8.
- [24] A. Jihad, A. A. N. Pratama, C. S. Yudha, M. Rahmawati, H. Widiyandari, and A. Purwanto, "Effect of Zn, Cu, and Mg doping on the structural characteristic of  $\text{LiNi}_0.6\text{Mn}_0.2\text{Co}_0.2\text{O}_2$  (NMC622)," in *ACM International Conference Proceeding Series Association for Computing Machinery*, 2020. DOI: 10.1145/3429789.3429857.
- [25] A. S. Wijareni, H. Widiyandari, A. Purwanto, A. F. Arif, and M. Z. Mubarak, "Morphology and particle size of a synthesized NMC 811 cathode precursor with mixed hydroxide precipitate and Nickel sulfate as Nickel sources and comparison of their electrochemical performances in an NMC 811 Lithium-ion battery," *Energies (Basel)*, vol. 15, no. 16, p. 5794, 2022. Doi: 10.3390/en15165794.
- [26] H. S. E. A. Gustiana, F. R. Agustiana, S. S. Nisa, and E. R. Dyartanti, "Synthesis and characterization of NMC 811 by oxalate and hydroxide coprecipitation method," *Evergreen*, vol. 9, no. 2, pp. 438-442, 2022. Doi: 10.5109/4794169.
- [27] D. Wang, I. Belharouak, G. Zhou, and K. Amine, "Synthesis of Lithium and Manganese-rich cathode materials via an oxalate co-precipitation method," *J Electrochem Soc*, vol. 160, no. 5, pp. A3108-A3112, 2013. Doi: 10.1149/2.016305jes.
- [28] H. Widiyandari, R. Ardiansah, and A. S. Wijareni, "Synthesis of lithium nickel manganese cobalt as cathode material for Li-ion battery using different precipitant agents by coprecipitation method," *AIP Conf Proc of the 2020 International Conference on Engineering and Information Technology for Sustainable Industry*, vol. 2217, pp. 030023-1-030023-8, 2020. DOI:10.1145/3429789.3429857.
- [29] S. S. Nisa, M. Rahmawati, C. S. Yudha, H. Nilasary, H. Nursukatmo, H. S. Oktaviano, S. U. Muzayanha, and A. Purwanto, "Fast approach to obtain layered transition-metal cathode material for rechargeable batteries," *Batteries*, vol. 8, no. 1, 2022. DOI: 10.3390/batteries8010004.
- [30] I. Jung, J. Choi, and Y. Tak, "Nickel oxalate nanostructures for supercapacitors," *J Mater Chem*, vol. 20, no. 29, pp. 6164-6169, 2010. DOI: 10.1039/c0jm00279h.
- [31] A. Habibi, M. Jalaly, R. Rahmanifard, and M. Ghorbanzadeh, "Solution combustion synthesis of the nanocrystalline NCM oxide for lithium-ion battery uses," *Mater Res Express*, vol. 5, no. 2, 2018. DOI: 10.1088/2053-1591/aaab12.
- [32] M. Satyanarayana, A. K. Jibin, E. Umeshbabu, J. James, and U. V. Varadaraju, "Optimizing conditions and improved electrochemical performance of layered  $\text{LiNi}_{1/3}\text{Co}_{1/3}\text{Mn}_{1/3}\text{O}_2$  cathode material for Li-ion batteries," *Ionics (Kiel)*, vol. 28, no. 1, pp. 229-240, 2022. DOI: 10.1007/s11581-021-04297-2.
- [33] R. Zhao, Z. Yang, J. Liang, D. Lu, C. Liang, X. Guan, A. Gao, and H. Chen,

- “Understanding the role of Na-doping on Ni-rich layered oxide  $\text{LiNi}_{0.5}\text{Co}_{0.2}\text{Mn}_{0.3}\text{O}_2$ ,” *J Alloys Compd*, vol. 689, pp. 318-325, 2016. DOI: 10.1016/j.jallcom.2016.07.230.
- [34] Z. Qiu, Y. Zhang, P. Dong, S. Xia, and Y. Yao, “A facile method for synthesis of  $\text{LiNi}_{0.8}\text{Co}_{0.15}\text{Al}_{0.05}\text{O}_2$  cathode material,” *Solid State Ion*, vol. 307, pp. 73-78, 2017. DOI: 10.1016/j.ssi.2017.04.011.
- [35] K. Meng, Z. Wang, H. Guo, and X. Li, “Enhanced cycling stability of  $\text{LiNi}_{0.8}\text{Co}_{0.1}\text{Mn}_{0.1}\text{O}_2$  by reducing surface oxygen defects,” *Electrochim Acta*, vol. 234, pp. 99-107, 2017. DOI: 10.1016/j.electacta.2017.03.054.
- [36] H. J. Noh, S. Youn, C. S. Yoon, and Y. K. Sun, “Comparison of the structural and electrochemical properties of layered  $\text{Li}[\text{Ni}_x\text{Co}_y\text{Mn}_z]\text{O}_2$  ( $x = 1/3, 0.5, 0.6, 0.7, 0.8$  and  $0.85$ ) cathode material for lithium-ion batteries,” *J Power Sources*, vol. 233, pp. 121-130, 2013. DOI: 10.1016/j.jpowsour.2013.01.063.
- [37] M. Zhang, J. Shen, J. Li, D. Zhang, Y. Yan, Y. Huang, and Z. Li, “Effect of micron-sized particle on the electrochemical properties of nickel-rich  $\text{LiNi}_{0.8}\text{Co}_{0.1}\text{Mn}_{0.1}\text{O}_2$  cathode materials,” *Ceram Int*, vol. 46, no. 4, pp. 4643-4651, 2020. DOI: 10.1016/j.ceramint.2019.10.195.
- [38] H. Gu, J. Wang, Z. Wang, J. Tong, N. Qi, G. Han, and M. Zhang, “Self-assembled porous  $\text{LiNi}_{0.8}\text{Co}_{0.1}\text{Mn}_{0.1}\text{O}_2$  cathode materials with micro/ nano-layered hollow morphologies for high-power lithium-ion batteries,” *Appl Surf Sci*, vol. 539, p. 148034, 2021. DOI: 10.1016/j.apsusc.2020.148034.